Archive of Applied Mechanics (2024) 94:1291–1311
https://doi.org/10.1007/s00419-024-02576-8

ORIGINAL

Büşra Uzun · Mustafa Özgür Yaylı · Ömer Civalek

Elastic medium and torsional spring effects on the nonlocal dynamic of functionally graded porous nanotubes

Received: 24 November 2023 / Accepted: 24 February 2024 / Published online: 4 April 2024

Abstract In this study, Eringen's nonlocal elasticity theory that applies the small size effects in functionally graded porous nanotubes embedded in an elastic matrix is discussed. The material properties of functionally graded porous nanotubes are taken into account to vary over the radius direction with a rule of mixture. The free torsional vibration relation according to nonlocal elasticity theory, via Hamilton's principle, is obtained and an eigenvalue solution is constructed for the free torsional vibration response of the presented work. The presented analytical model is validated by comparing the calculated mathematical results for homogeneous nanotubes with rigid and non-rigid boundary conditions. Special attention is given to deformable boundary conditions, porosity coefficient, material grading coefficient and also to the influence of elastic medium on the free torsional vibration frequencies. In this paper, it has been proven that the influence of length, elastic medium, elastic torsional spring rigidities, material grading and porosity coefficients on the vary in the torsional vibration frequency of the functionally graded nanotube is not small.

Keywords Elastic medium · Porosity · Torsional spring · Functionally graded material · Nonlocality

1 Introduction

Functionally graded material (FGM) belongs to a class of advanced composites whose properties vary along one or more specific directions. These composites, formed by a smooth transition of at least two different materials, are used to eliminate sharp interfaces frequently encountered in layered composite materials [1]. FGMs, which replace the mentioned sharp interfaces with gradient interfaces that provide a smooth transition, have a unique feature in terms of having the ability to design a material for a specific application [2, 3]. Functionally graded composites can also be found in porous form. Although these pores are considered as production defects in some academic studies, the ability of porous structures to be specially shaped to increase performance attracts attention [4]. The morphology of the pores is related to the unusual chemical, mechanical, thermal, electronic and biological properties of the structure in which they are located, and is therefore remarkable [4]. In addition to the fact that the most distinctive feature of porous materials is their low weight, as well as being very successful in terms of insulation. Nowadays, porous materials are becoming more and more popular due to the importance of material properties such as recyclability and processability. The new materials are attracting attention in the world literature as applications of aerospace, space and advanced engineering mechanics.

B. Uzun (✉) · M. Ö. Yaylı
Department of Civil Engineering, Engineering Faculty, Bursa Uludag University, Görükle Campus, 16059 Bursa, Turkey
e-mail: buzun@uludag.edu.tr

Ö. Civalek
Department of Civil Engineering, Engineering Faculty, Akdeniz University, Antalya, Turkey

Ö. Civalek
Department of Medical Research, China Medical University Hospital, China Medical University, Taichung, Taiwan

The specific gravity of these new materials with hollow and especially FGM-based hollow structures is very low and have various advantages such as sufficient absorption capacity and very low electrical and thermal conductivity.

The classical elastic models are not sufficient to define the mechanical response of small-sized structures. The small-size effects can be recognized to become much more prominent as the lengths of these structures reach the nano-scales. The classical elasticity theories (CET) cause some deficits in defining nano-sized structures. Consequently, some higher-order elasticity theories have been presented to take into account different small-size effects, for example: strain gradient theory [5, 6], strain gradient nonlocal theory [7], Eringen's nonlocal elasticity theory (NLET) in differential form [8–10], modified couple stress theory [11] and couple stress theory [12]. There are several studies describing the mechanical response of various micro/nano-sized elements based on the NLET [13–26]. This theory takes into account the softening effect found in micro/nano-sized structures. Different studies [27, 28] have been presented the analyses of small-size elements via nonlocal and strain gradient effects (strain gradient nonlocal theory) which define both softening and hardening effects in micro/nano-sized structures. Also, in order to study small-size effects of micro/nano-sized structures couple stress and modified couple stress theories have been utilized by many scholars [29–35]. Kiani [36] has researched the vibration response of nano-sized plates under moving particles by using Eringen's NLET. Shirai et al. [37, 38] have studied and manufactured the first nano-machines. It has been realized that the method studied and the results obtained are promising, and light has been shed on new studies. After that, Morin et al. [39] have studied a novel nano-vehicle with a synthetic molecular motor powered by light. Arani et al. [40] have studied the effect of small-size parameters on the dynamical response of single-walled boron nitride nanotubes (NTs) under a moving nanoparticle via a nonlocal piezo elasticity theory. By using molecular dynamics simulation [41–44] have investigated mechanical responses of carbon-based structures. In addition, using molecular mechanics, Lu et al. [45] have investigated a double-walled carbon NT in a thermal environment under static stability. They have shown that the thermal influences decrease the buckling load of the double-walled carbon NTs. As is well-known, working with molecular dynamics models requires large computer memories and a lot of time to perform the analyses. In recent years, there have been so many works that can perform mechanical analyses with higher-order elasticity theories that, as can be appreciated, it is not possible to give all of them in a literature review. Here a limited number of works that have been solved with some higher-order elasticity theories that caught the author's eye are listed. Some of these works can be listed here. Aydogdu and Filiz [46] have explored the axial dynamic analysis of the single-walled carbon NT-based mass sensor based on Eringen's NLET. The influences of the different lengths, small-scale parameters and attached mass have been investigated. In another study, Aydogdu [47] has investigated the longitudinal vibration of double-walled carbon NTs based on the Eringen's NLET including the van der Waals force. On the other hand, Natsuki et al. [48] have explored the frequency shifts of the clamped carbon nanotube. Song et al. [49] have investigated the vibrations of FG composite plates with a direct approximation. They have investigated the impacts of weight function, size effects and geometry in addition to the number of layers. A dynamic analysis with the force function of a double-nanoplate system made of orthotropic material has been studied by Atanasov et al. [50]. Various mathematical methods are used, especially in the macro sizes, as a basis for studies at the microscale.

As can be understood, the mechanical response of nano/micro-scale elements has gained much interest from scholars. The unique properties of nano/microelements, combined with the functionally graded form, enable extraordinary performances. Functionally graded composite materials, in which at least two different materials come together and exhibit more advanced properties, can also contain pores in their cross-sections. We have recently come across articles [27, 28, 33, 35] in the literature in which such materials are considered for various elements at the nano/micro scale and their mechanical responses are investigated. Uzun and Yaylı [33] have studied the torsional vibration of restrained FG porous NTs via modified couple stress theory. Civalek et al. [14] have explored the vibrational frequencies of FG nonlocal nanotubes restrained with elastic springs. Li and Hu [51] have introduced the torsional vibration analyses of two-directional FG non-porous NTs based on the NLET. Also, the torsional dynamic of bi-directional FG microtubes has been explored by Li and Hu [52] via modified couple stress theory.

In this paper, the free torsional vibration response of embedded FG porous NTs is studied based on NLET. The functional porous material is considered to be graded through radial direction with a material distribution. The boundary conditions and equation of motion are obtained, employing the Hamilton principle. Afterward, a Fourier infinite series and Stokes' transformation are applied to construct an eigenvalue problem to obtain the free torsional frequencies of FG porous NTs. Various examples are solved to compare the results of the presented model with those predicted by different studies. The obtained results show that the material porosity

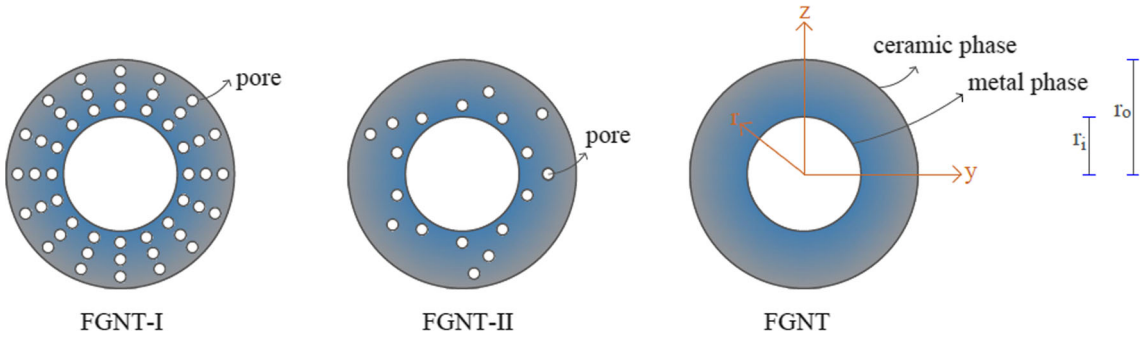

Fig. 1 Cross-sections of functionally graded composite nanotubes

with elastic boundaries has a significant effect on the dynamical response of the functionally graded porous nanotube. The mathematical values presented in this study can provide useful guidelines for developing and designing FG porous NTs based on nanomachines.

2 Material distributions of functionally graded tubes

Figure 1 shows nanotubes consisting of functionally graded porous/non-porous composite materials with ceramic phases on the outer surface and metal phases on the inner surface. FG nanotubes with pores are considered in two different forms. Functionally graded composite nanotubes with pores homogeneously (evenly) distributed along the radius are named "FGNT-I". Functionally graded composite nanotubes with pore distribution varying along the radius are named "FGNT-II". Finally, functionally graded composite nanotubes without pores in the cross-section are named "FGNT". For functionally graded composite NTs, the material properties are considered to be distributed along the radius direction by a function called the power-law. Based on this function, the volume ratios of ceramic and metal components in the radius direction can be written as follows, respectively [53, 54]:

$$V_c(r) = \left(\frac{r - r_i}{r_o - r_i}\right)^p \tag{1}$$

$$V_m(r) = 1 - \left(\frac{r - r_i}{r_o - r_i}\right)^p \tag{2}$$

where, $V_m(r)$ and $V_c(r)$ are the volume ratios of the metal and ceramic phases that form the composite NT, while r represents the radius direction. Furthermore, p is the material grading coefficient, while r_o and r_i are the outer and inner radius values, respectively. The material grading coefficient p is expressed in the range $p \in [0, \infty)$. In conjunction with the rule of mixture, any effective material property of the FG composite with pores in the cross-section is written as follows [53, 55–57]:

$$F(r) = F_c\left(V_c(r) - \frac{\overline{\vartheta}}{2}\right) + F_m\left(V_m(r) - \frac{\overline{\vartheta}}{2}\right) \tag{3}$$

In Eq. (3), F represents any effective material property of the functionally graded composite such as Young's modulus (modulus of elasticity) E, Poisson's ratio ν, shear modulus μ, and mass density ρ. F_m and F_c denote any material properties of metal and ceramic phases, respectively. Finally, $\overline{\vartheta}$ is the porosity function. The porosity functions $\overline{\vartheta}$ for FGNT-I and FGNT-II, respectively, are expressed as follows:

$$\overline{\vartheta}(r) = \vartheta, \text{constant} \tag{4}$$

$$\overline{\vartheta}(r) = \vartheta\left(1 - \frac{r - r_i}{r_o - r_i}\right) \tag{5}$$

In the above equations, ϑ $(0 \leq \vartheta \ll 1)$ is the porosity ratio (porosity coefficient). With the porosity function in Eq. (4) and rule of the mixture), the effective material property expression for FGNT-I is calculated as follows [54]:

$$F(r) = (F_c - F_m)\left(\frac{r - r_i}{r_o - r_i}\right)^p + F_m - \frac{\vartheta}{2}(F_c + F_m) \tag{6}$$

Similarly, with the porosity function in Eq. (5) and rule of mixture, the effective material property expression for FGNT-II is obtained as follows [54]:

$$F(r) = (F_c - F_m)\left(\frac{r - r_i}{r_o - r_i}\right)^p + F_m - \frac{\vartheta}{2}(F_c + F_m)\left(1 - \frac{r - r_i}{r_o - r_i}\right) \tag{7}$$

If ϑ is set to zero in Eqs. (6 and 7), we see that these porosity-dependent expressions reduce to $F(r)$ of FG non-porous nanotubes as follows:

$$F(r) = (F_c - F_m)\left(\frac{r - r_i}{r_o - r_i}\right)^p + F_m \tag{8}$$

Based on the equations given above, the effective moduli of elasticity for porous FGNT-I, porous FGNT-II and non-porous FGNT are calculated as follows, respectively:

$$E(r) = (E_c - E_m)\left(\frac{r - r_i}{r_o - r_i}\right)^p + E_m - \frac{\vartheta}{2}(E_c + E_m) \tag{9}$$

$$E(r) = (E_c - E_m)\left(\frac{r - r_i}{r_o - r_i}\right)^p + E_m - \frac{\vartheta}{2}(E_c + E_m)\left(1 - \frac{r - r_i}{r_o - r_i}\right) \tag{10}$$

$$E(r) = (E_c - E_m)\left(\frac{r - r_i}{r_o - r_i}\right)^p + E_m \tag{11}$$

As can be understood, the material properties for FGNT and FGNT-I are constant in the $p = 0$ case. In the case of $p = 0$ for FGNT, the nanotube has homogeneous material properties consisting only of ceramic material. For FGNT-I, in the $p = 0$ case, the composite nanotube properties are constant but closer to the ceramic properties. Also, in Fig. 2, the variation of Young's modulus of functionally graded nanotubes is plotted for various material grading coefficients with respect to r/r_i. $E_c = 151$ GPa, $E_m = 70$ GPa, $\vartheta = 0.1$ values are used in the graphs in Fig. 2.

Based on the Eqs. (6–8), we can write the grading formulas of other material properties of FG porous/non-porous nanotubes. Mass density $\rho(r)$ relations can be written as follows:

$$\rho(r) = (\rho_c - \rho_m)\left(\frac{r - r_i}{r_o - r_i}\right)^p + \rho_m - \frac{\vartheta}{2}(\rho_c + \rho_m) \tag{12}$$

$$\rho(r) = (\rho_c - \rho_m)\left(\frac{r - r_i}{r_o - r_i}\right)^p + \rho_m - \frac{\vartheta}{2}(\rho_c + \rho_m)\left(1 - \frac{r - r_i}{r_o - r_i}\right) \tag{13}$$

$$\rho(r) = (\rho_c - \rho_m)\left(\frac{r - r_i}{r_o - r_i}\right)^p + \rho_m \tag{14}$$

Poisson's ratios of composite nanotubes $\upsilon(r)$ can be calculated by:

$$\upsilon(r) = (\upsilon_c - \upsilon_m)\left(\frac{r - r_i}{r_o - r_i}\right)^p + \upsilon_m - \frac{\vartheta}{2}(\upsilon_c + \upsilon_m) \tag{15}$$

$$\upsilon(r) = (\upsilon_c - \upsilon_m)\left(\frac{r - r_i}{r_o - r_i}\right)^p + \upsilon_m - \frac{\vartheta}{2}(\upsilon_c + \upsilon_m)\left(1 - \frac{r - r_i}{r_o - r_i}\right) \tag{16}$$

$$\upsilon(r) = (\upsilon_c - \upsilon_m)\left(\frac{r - r_i}{r_o - r_i}\right)^p + \upsilon_m \tag{17}$$

Lastly, relations for shear modulus $\mu(r)$ are defined by:

$$\mu(r) = \frac{(E_c - E_m)\left(\frac{r - r_i}{r_o - r_i}\right)^p + E_m - \frac{\vartheta}{2}(E_c + E_m)}{2\left(1 + \left[(\upsilon_c - \upsilon_m)\left(\frac{r - r_i}{r_o - r_i}\right)^p + \upsilon_m - \frac{\vartheta}{2}(\upsilon_s + \upsilon_m)\right]\right)} \tag{18}$$

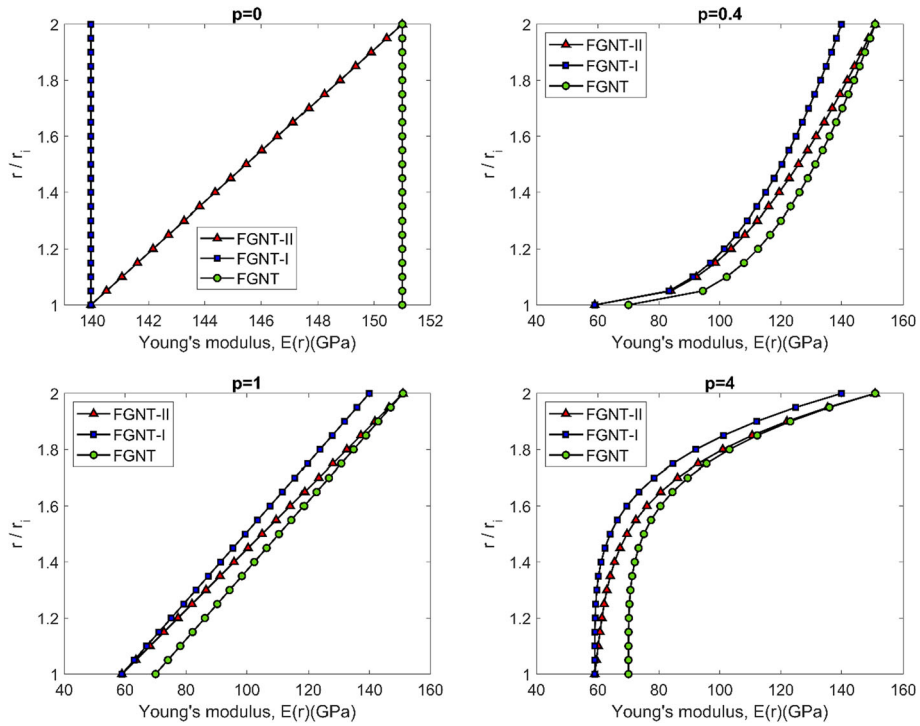

Fig. 2 Variations of modulus of elasticity of functionally graded composite nanotubes with respect to r/r_i

$$\mu(r) = \frac{(E_c - E_m)\left(\frac{r-r_i}{r_o-r_i}\right)^p + E_m - \frac{\vartheta}{2}(E_c + E_m)\left(1 - \frac{r-r_i}{r_o-r_i}\right)}{2\left(1 + \left[(\upsilon_c - \upsilon_m)\left(\frac{r-r_i}{r_o-r_i}\right)^p + \upsilon_m - \frac{\vartheta}{2}(\upsilon_c + \upsilon_m)\left(1 - \frac{r-r_i}{r_o-r_i}\right)\right]\right)} \tag{19}$$

$$\mu(r) = \frac{(E_c - E_m)\left(\frac{r-r_i}{r_o-r_i}\right)^p + E_m}{2\left(1 + \left[(\upsilon_c - \upsilon_m)\left(\frac{r-r_i}{r_o-r_i}\right)^p + \upsilon_m\right]\right)} \tag{20}$$

The above relations include the calculation of all the properties that will be required for the solution in this study.

3 Nonlocal torsional vibration

In this part, the main relations of the NLET presented by Eringen and the process steps to obtain the torsional vibration problem are briefly presented. In the literature, torsional vibration analysis of homogeneous bar/rod models with solid circular cross-sections has been widely studied, while analysis of FG composite hollow tubes is rare. However, the torsional vibration of FG porous NTs in an elastic medium at elastic boundaries, which will be presented in this study, has not been studied before. Figure 3 shows the embedded FG nanotube with L length in an elastic matrix and at deformable boundaries.

The constitutive equations of the NLET are given by Eringen [10] as follows:

$$\sigma_{ij,i} + \rho(r)\left(\varkappa_j - \frac{\partial^2 u_j}{\partial t^2}\right) = 0 \tag{21}$$

$$\sigma_{ij,i} = \int_V \alpha\left(\left|x' - x\right|, \varsigma\right)\sigma_{ij} dV\left(x'\right) \tag{22}$$

$$\sigma_{ij} = \lambda(r)\varepsilon_{kk}\delta_{ij} + 2\mu(r)\varepsilon_{ij} \tag{23}$$

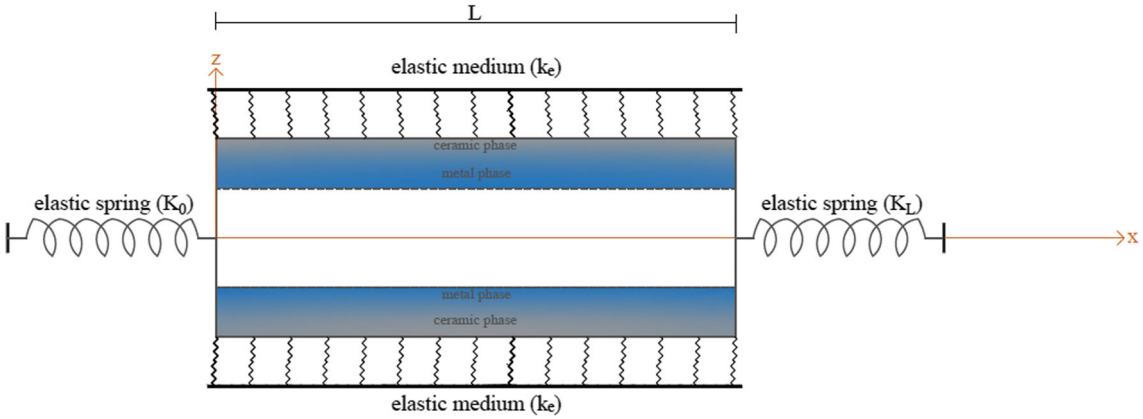

Fig. 3 FG nanotube in an elastic medium and at deformable boundaries

$$\varepsilon_{ij} = \frac{1}{2}\left(\frac{\partial u_i}{\partial x_j^{'}} + \frac{\partial u_j}{\partial x_i^{'}}\right) \tag{24}$$

In the above equations, $\sigma_{ij,i}$ is the NL stress tensor, $\varkappa_j$ is the mass force density, t is time and u_j is the displacement vector at the reference point. σ_{ij} represents the classical (local) stress tensor, while $\alpha(|x\prime - x|, \varsigma)$ is the nonlocal kernel function and V is the volume. $|x\prime - x|$ is the distance between points x and $x\prime$, ε_{ij} is the linear strain tensor at any point and δ_{ij}(δ_{ij}=1 for i=j, δ_{ij}=0 for i≠j) is the Kronecker delta function. Furthermore, $\lambda(r)$ and $\mu(r)$ are Lame constants and are written as follows:

$$\lambda(r) = \frac{E(r)\nu(r)}{(1+\nu(r))(1-2\nu(r))} \tag{25}$$

$$\mu(r) = \frac{E(r)}{2(1+\nu(r))} \tag{26}$$

Moreover, the parameter in the nonlocal kernel function in Eq. (22) is denoted as $\varsigma = \frac{e_0 a}{L}$ and $\alpha(|x\prime - x|)$ is the nonlocal modulus with length-3 unit [10]. It follows that the nonlocal modulus will depend on a characteristic length ratio, $a/\overline{L}$. Here, a is the characteristic internal length, while $\overline{L}$ is the characteristic external length. Examples of the characteristic internal length are the particle size and the distance between carbon bonds, while the characteristic external length, the crack length and the length of the nanostructure are examples [58]. e_0 is a constant that can be determined experimentally for the material [10]. $e_0 a$ is called the nonlocal parameter.

It is stated that it is very difficult to analyze elasticity problems with the integral constitutive relation given in Eq. (22). As a result, an equivalent differential form of the expression given in Eq. (22) was developed to analyze different problems [59]. Moreover, the differential form, which provides a simpler solution compared to the integral form, is widely used in nanostructures [60]. Stress relations for the NL constitutive equation were proposed by Eringen [9] as follows:

$$\left(1 - (e_0 a)^2 \frac{\partial^2}{\partial x^2}\right)\sigma_{ij,i} = \sigma_{ij} \tag{27}$$

$$\left(1 - (e_0 a)^2 \frac{\partial^2}{\partial x^2}\right)\tau_{ij,i} = \tau_{ij} \tag{28}$$

Torsion of hollow tubes, both composite and non-composite, has attracted the interest of many researchers due to the high strength and stiffness of these elements in torsion. Torsional analysis of FG composite tubes, which have their place in the practical use of modern structures, biomechanical and aeronautical applications, has received much attention [61]. Cylindrical shafts subjected to static torque and torsional vibrations have an important place in engineering. Moreover, laboratory tests apply torsional vibration to determine the shear modulus of the material, which is required as one of the basic parameters in most engineering design problems [62]. In order to present a simple model to explain the size-dependent static behavior of FG porous and nonporous composite nanotubes subjected to torsion, the following assumptions are considered throughout the study [52]:

(i) When a hollow circular nanotube made of FG composite material, whose properties vary with the radius, is subjected to torsion, each cross-section remains plane and intact.
(ii) The functionally graded composite material has a linear elastic stress–strain relation obeying Hooke's law.
(iii) Stresses do not exceed the limit of proportionality.
(iv) The cross-section of the composite nanotubes is the same along its length.
(v) Composite NTs can be modeled on the basis of the NLET formulations.

In this study, Hamilton's technique is used to obtain the governing equations for vibration problems. Hamilton's principle is expressed in the time domain $[t_1, t_2]$ as follows [63]:

$$\delta \int_{t_1}^{t_2} (U - K - \Lambda) \mathrm{d}t = 0 \tag{29}$$

Here, δ is the variation operator.U, K and Λ represent the nanotube's strain and kinetic energies, also work done by external loads, respectively. The kinetic energy of the composite nanotube is written as follows [51]:

$$K = \frac{1}{2} \int_0^L \int_A \rho(r) \left[\left(\frac{\partial u_x}{\partial t} \right)^2 + \left(\frac{\partial u_y}{\partial t} \right)^2 + \left(\frac{\partial u_z}{\partial t} \right)^2 \right] \mathrm{d}A\mathrm{d}x = \frac{1}{2} \int_0^L \rho^J \left(\frac{\partial \theta(x,t)}{\partial t} \right)^2 \mathrm{d}x \tag{30}$$

where, u_x, u_y and u_z define the linear motion components in the x, y and z directions, respectively. A denotes the cross-sectional area, $\theta(x, t)$ is torsion angle. ρ^J is the mass polar moment of inertia of the composite nanotube and is calculated as follows:

$$\rho^J = 2\pi \int_{r_i}^{r_0} \rho(r) r^3 \mathrm{d}r \tag{31}$$

In the case of linearized elastic material, the strain energy due to nonlocal elasticity for composite nanotube made of functionally graded material can be given as [51]:

$$U = \int_V \left(2\sigma_{xy}\varepsilon_{xy} + 2\sigma_{xz}\varepsilon_{xz} \right) \mathrm{d}V \tag{32}$$

For simplicity, if the stresses are expressed in terms of torque (M_b) as follows [51]:

$$M_b = \int_A \left(y\sigma_{xz} - z\sigma_{xy} \right) \mathrm{d}A \tag{33}$$

is written. With the nonlocal constitutive equation and strain expressions, the following equation can be established [51]:

$$M_b - (e_0 a)^2 \frac{\partial^2 M_b}{\partial x^2} = \mu^J \frac{\partial \theta(x,t)}{\partial x} \tag{34}$$

Here, μ^J is the shear stiffness of the composite nanotube and is calculated as follows:

$$\mu^J = 2\pi \int_{r_i}^{r_0} \mu(r) r^3 \mathrm{d}r \tag{35}$$

In this problem, as mentioned before, the composite nanotube is considered to be in an elastic medium. The work done by the medium surrounding the composite nanotube is written as follows [64]:

$$\Lambda = -\int_0^L k_e \theta(x,t)^2 \mathrm{d}x \tag{36}$$

Here, k_e is the stiffness of the elastic medium surrounding the composite NT. Inserting the first variations of the K, U and Λ given above into Eq. (34) and performing partial integration, the following equation of motion is obtained:

$$\frac{\partial M_b}{\partial x} - k_e\theta(x,t) - \rho^J \frac{\partial^2\theta(x,t)}{\partial t^2} = 0 \tag{37}$$

If the expression obtained above is differentiated once and substituted in Eq. (34), the torque based on the NLET is derived as follows [13]:

$$M_b = (e_0a)^2 k_e \frac{\partial\theta(x,t)}{\partial x} + (e_0a)^2\rho^J \frac{\partial^3\theta(x,t)}{\partial x\partial t^2} + \mu^J \frac{\partial\theta(x,t)}{\partial x} \tag{38}$$

If the derived torque expression is differentiated once and substituted in Eq. (37), the equation governing the torsional vibration of composite NTs based on the NLET is established as follows [13]:

$$\mu^J \frac{\partial^2\theta(x,t)}{\partial x^2} - k_e\theta(x,t) - \rho^J \frac{\partial^2\theta(x,t)}{\partial t^2} + (e_0a)^2 k_e \frac{\partial^2\theta(x,t)}{\partial x^2} + (e_0a)^2\rho^J \frac{\partial^4\theta(x,t)}{\partial x^2\partial t^2} = 0 \tag{39}$$

The equation above includes the effect of the elastic medium together with nonlocal effects. If $k_e = 0$ taken in this equation, the effect of the elastic medium is removed from the problem.

4 Fourier series based solution for FG porous nanotubes

When we look at the literature, it is easy to see that various approaches have been adopted by researchers [65–74] such as finite difference and element methods, quadrature techniques, and state-space approach for solving a problem. The type of problem, boundary and external load conditions are important for the selection of the appropriate approach. Since the effect of elastic boundary conditions will be investigated in this study, a solution approach based on the Fourier sine series and Stokes' transform is used to construct a general eigenvalue problem. As it is known, eigenvalue problems are used in mechanics to find a value that takes displacements to infinity at once, that is, a value that brings two or more equilibrium systems to the same point. Physically, this can sometimes be buckling load and sometimes be vibration frequency. In various branches of engineering, eigenvalues correspond to different parameters. Here, a 2×2 eigenvalue problem has been constructed by defining the displacement function separately in the boundary conditions and in the region. To obtain the nontrivial solution, the determinant of the coefficients matrix obtained at the end is made zero. When we look at the studies on torsional vibration of homogeneous or FG nanorods, we see that most of them investigate rigid (cantilevered or clamped) boundary conditions. Our aim in this paper is to present a solution that can study the torsional vibration frequencies of FG composite tubes with pores in the cross-section and in an esthetic center under general (both rigid and non-rigid) boundary conditions. As a first step, the partial differential equation in Eq. (39) is written as an ordinary differential equation with the help of $\theta(x,t) = \varphi(x)e^{i\omega t}$ as follows:

$$\mu^J \frac{d^2\varphi(x)}{dx^2} - k_e\varphi(x) + \omega^2\rho^J\varphi(x) + (e_0a)^2 k_e \frac{d^2\varphi(x)}{dx^2} - \omega^2(e_0a)^2\rho^J \frac{d^2\varphi(x)}{dx^2} = 0 \tag{40}$$

Here, $\varphi(x)$ is the torsion angle function (modal function) and ω is the angular frequency. In the adopted solution method, the torsion angle is considered to be defined as a constant at both ends of the tube ($\varphi(x) = \varphi_0 \text{for} x = 0 \text{and} \varphi(x) = \varphi_L \text{for} x = L$) and as a sine function in the intermediate region as follows [30]:

$$\varphi(x) = \sum_{n=1}^{\infty} B_n \sin\left(\frac{n\pi x}{L}\right), 0 < x < L \tag{41}$$

In the above expression, n is the number of terms and B_n is the Fourier coefficient. Details of the intermediate steps of the solution based on the combination of Fourier sine series and Stokes' transform can be found in a number of works [14, 16, 17, 30] in the literature. The ordinary differential equations representing the problems solved by these studies have different orders. The problem in this paper is, understandably, expressed by a second-order differential equation and the following two derivatives are sufficient for the solution [30]:

$$\frac{d\varphi(x)}{dx} = \frac{\varphi_L - \varphi_0}{L} + \sum_{n=1}^{\infty}\left(\frac{2\left((-1)^n\varphi_L - \varphi_0\right)}{L} + \frac{n\pi}{L}B_n\right)\cos\left(\frac{n\pi x}{L}\right) \tag{42}$$

$$\frac{d^2\varphi(x)}{dx^2} = -\sum_{n=1}^{\infty} \frac{n\pi}{L}\left(\frac{2\left((-1)^n\varphi_L - \varphi_0\right)}{L} + \frac{n\pi}{L}B_n\right)\sin\left(\frac{n\pi x}{L}\right) \tag{43}$$

If Eqs. (41–43) are substituted in Eq. (40):

$$\sum_{n=1}^{\infty}\left[\left(\mu^J + (e_0a)^2k_e - \omega^2(e_0a)^2\rho^J\right)\left(-\frac{n\pi}{L}\left(\frac{2\left((-1)^n\varphi_L - \varphi_0\right)}{L} + \frac{n\pi}{L}B_n\right)\right) + \left(\omega^2\rho^J - k_e\right)B_n\right]\sin\left(\frac{n\pi x}{L}\right) = 0 \tag{44}$$

is obtained. When this equation is solved, the Fourier coefficient B_n is found as follows:

$$B_n = \frac{2n\pi(\mu^J + (e_0a)^2(k_e - \rho^J\omega^2))\varphi_0}{\mu^J n^2\pi^2 + (L^2 + n^2\pi^2(e_0a)^2)(k_e - \rho^J\omega^2)} - \frac{2(-1)^n n\pi(\mu^J + (e_0a)^2(k_e - \rho^J\omega^2))\varphi_L}{\mu^J n^2\pi^2 + (L^2 + n^2\pi^2(e_0a)^2)(k_e - \rho^J\omega^2)} \tag{45}$$

After calculating the Fourier coefficient, the equation that allows us to calculate the torsion angle is obtained as follows:

$$\varphi(x) = \sum_{n=1}^{\infty}\left(\frac{2n\pi(\mu^J + (e_0a)^2(k_e - \rho^J\omega^2))\varphi_0}{\mu^J n^2\pi^2 + (L^2 + n^2\pi^2(e_0a)^2)(k_e - \rho^J\omega^2)} - \frac{2(-1)^n n\pi(\mu^J + (e_0a)^2(k_e - \rho^J\omega^2))\varphi_L}{\mu^J n^2\pi^2 + (L^2 + n^2\pi^2(e_0a)^2)(k_e - \rho^J\omega^2)}\right)\sin\left(\frac{n\pi}{L}x\right) \tag{46}$$

The above equation is the static equation for torsion. Thus, when the desired parameters are substituted in the above equation, the torsion angle of the FG porous nanotubes is found. Now, the eigenvalue problem of the solution based on Fourier sine series and Stokes' transform will be obtained. For this, the torsional moment of the nonlocal composite nanotube is equal to the product of the torsion spring and the torsion function. Thus, the following equations are established for end points of the nonlocal composite nanotube:

$$(e_0a)^2k_e\frac{\partial\theta(x,t)}{\partial x} + (e_0a)^2\rho^J\frac{\partial^3\theta(x,t)}{\partial x\partial t^2} + \mu^J\frac{\partial\theta(x,t)}{\partial x}|_{x=0} = K_0\varphi_0 \tag{47}$$

$$(e_0a)^2k_e\frac{\partial\theta(x,t)}{\partial x} + (e_0a)^2\rho^J\frac{\partial^3\theta(x,t)}{\partial x\partial t^2} + \mu^J\frac{\partial\theta(x,t)}{\partial x}|_{x=0} = -K_L\varphi_L \tag{48}$$

Here, K_0 and K_L are the stiffnesses of the deformable torsional springs at the $x = 0$ ends and x=L ends of the composite nanotubes, respectively. Equations (47 and 48) give the following two sets of equations:

$$\left(-K_0 + \frac{(e_0a)^2\rho^J\omega^2}{L} - \frac{(e_0a)^2k_e}{L} - \frac{\mu^J}{L} - \sum_{n=1}^{\infty}\frac{2L(k_e - \rho^J\omega^2)(\mu^J + (e_0a)^2(k_e - \rho^J\omega^2))}{\mu^J n^2\pi^2 + k_e(L^2 + n^2\pi^2(e_0a)^2) - (L^2 + n^2\pi^2(e_0a)^2)\rho^J\omega^2}\right)\varphi_0 + \left(-\frac{(e_0a)^2\rho^J\omega^2}{L} + \frac{(e_0a)^2k_e}{L} + \frac{\mu^J}{L} + \sum_{n=1}^{\infty}\frac{2(-1)^n L(k_e - \rho^J\omega^2)(\mu^J + (e_0a)^2(k_e - \rho^J\omega^2))}{\mu^J n^2\pi^2 + k_e(L^2 + n^2\pi^2(e_0a)^2) - (L^2 + n^2\pi^2(e_0a)^2)\rho^J\omega^2}\right)\varphi_L = 0 \tag{49}$$

$$\left(-\frac{(e_0a)^2\rho^J\omega^2}{L} + \frac{(e_0a)^2k_e}{L} + \frac{\mu^J}{L} + \sum_{n=1}^{\infty}\frac{2(-1)^n L(k_e - \rho^J\omega^2)(\mu^J + (e_0a)^2(k_e - \rho^J\omega^2))}{\mu^J n^2\pi^2 + k_e(L^2 + n^2\pi^2(e_0a)^2) - (L^2 + n^2\pi^2(e_0a)^2)\rho^J\omega^2}\right)\varphi_0 + \left(-K_L + \frac{(e_0a)^2\rho^J\omega^2}{L} - \frac{(e_0a)^2k_e}{L} - \frac{\mu^J}{L} - \sum_{n=1}^{\infty}\frac{2L(k_e - \rho^J\omega^2)(\mu^J + (e_0a)^2(k_e - \rho^J\omega^2))}{\mu^J n^2\pi^2 + k_e(L^2 + n^2\pi^2(e_0a)^2) - (L^2 + n^2\pi^2(e_0a)^2)\rho^J\omega^2}\right)\varphi_L = 0 \tag{50}$$

This set of two equations can also be set up as an eigenvalue problem as follows:

$$\begin{bmatrix} Z_{11} & Z_{12} \\ Z_{21} & Z_{22} \end{bmatrix} \begin{bmatrix} \varphi_0 \\ \varphi_L \end{bmatrix} = 0 \tag{51}$$

To find the frequencies of the composite nanotube, we need to set the determinate of the matrix of coefficients equal to zero and obtain the eigenvalues. That is,

$$\begin{vmatrix} Z_{11} & Z_{12} \\ Z_{21} & Z_{22} \end{vmatrix} = 0 \tag{52}$$

equation needs to be solved and its eigenvalues found. The four elements of the matrix given Eq. (52) are defined by:

$$Z_{11} = -K_0 + \frac{(e_0a)^2\rho^J\omega^2}{L} - \frac{(e_0a)^2k_e}{L} - \frac{\mu^J}{L} - \sum_{n=1}^{\infty} \frac{2L(k_e - \rho^J\omega^2)(\mu^J + (e_0a)^2(k_e - \rho^J\omega^2))}{\mu^J n^2\pi^2 + k_e(L^2 + n^2\pi^2(e_0a)^2) - (L^2 + n^2\pi^2(e_0a)^2)\rho^J\omega^2} \tag{53}$$

$$Z_{12} = -\frac{(e_0a)^2\rho^J\omega^2}{L} + \frac{(e_0a)^2k_e}{L} + \frac{\mu^J}{L} + \sum_{n=1}^{\infty} \frac{2(-1)^n L(k_e - \rho^J\omega^2)(\mu^J + (e_0a)^2(k_e - \rho^J\omega^2))}{\mu^J n^2\pi^2 + k_e(L^2 + n^2\pi^2(e_0a)^2) - (L^2 + n^2\pi^2(e_0a)^2)\rho^J\omega^2} \tag{54}$$

$$Z_{21} = -\frac{(e_0a)^2\rho^J\omega^2}{L} + \frac{(e_0a)^2k_e}{L} + \frac{\mu^J}{L} + \sum_{n=1}^{\infty} \frac{2(-1)^n L(k_e - \rho^J\omega^2)(\mu^J + (e_0a)^2(k_e - \rho^J\omega^2))}{\mu^J n^2\pi^2 + k_e(L^2 + n^2\pi^2(e_0a)^2) - (L^2 + n^2\pi^2(e_0a)^2)\rho^J\omega^2} \tag{55}$$

$$\begin{aligned} Z_{22} = -K_L + \frac{(e_0a)^2\rho^J\omega^2}{L} - \frac{(e_0a)^2k_e}{L} - \frac{\mu^J}{L} \\ - \sum_{n=1}^{\infty} \frac{2L(k_e - \rho^J\omega^2)(\mu^J + (e_0a)^2(k_e - \rho^J\omega^2))}{\mu^J n^2\pi^2 + k_e(L^2 + n^2\pi^2(e_0a)^2) - (L^2 + n^2\pi^2(e_0a)^2)\rho^J\omega^2} \end{aligned} \tag{56}$$

At the boundaries, the displacement parameters defined differently are substituted in the force boundary conditions and a matrix of coefficients including elastic medium, deformable torsional springs, nonlocal parameter, geometric properties, shear modulus and mass density with FGM and pore properties is formed. To obtain a non-trivial solution of Eq. (52), determinant of the coefficient matrix should be zero. Also, if the k_e's are set equal to zero, the nonlocal problem becomes independent of the elastic medium effect.

5 Numerical results

This section of this paper first presents the validation studies. The correctness of the solution approach presented in this paper is proved by a study found in the literature. Numanoğlu and Civalek [13] presented the torsional vibration of embedded homogeneous nanorods with respect to NLET with analytical and finite element solutions. In the study, the authors studied five different boundary conditions. These boundary conditions are as follows: clamped at both ends, cantilever, free at both ends, clamped at one end and spring-attached at the other end, and free at one end and spring-attached at the other end. The material properties and geometrical properties used in the comparison studies are as follows: $E = 1000$ GPa,$\rho = 1340\text{kg/m}^3$,$\upsilon = 0.27$, $r_i = 2.48$nm, $r_o = 2.82$nm, $L = 20$nm. Also, as can be seen from the tables, the frequencies are in dimensionless form and the dimensionless parameters used for the comparison studies are given as follows [13]:

$$\overline{\omega} = \omega L\sqrt{\frac{\rho}{\mu}} \tag{57}$$

Table 1 Comparison of non-dimensional frequencies for embedded homogeneous clamped rods ($\overline{k_e}$=10)

e_0a (nm)	Mode number	Ref. [13]		This study	This study
		Exact	FE	$n = 10$	$n = 20$
1	1	4.4308	4.4322	4.4308	4.4308
	2	6.7773	6.7900	6.77732	6.77732
	3	9.0932	9.1319	9.09315	9.09315
2	1	4.3570	4.3589	4.35695	4.35695
	2	6.1890	6.1977	6.18905	6.18905
	3	7.5526	7.5721	7.55257	7.55257

Table 2 Comparison of non-dimensional frequencies for embedded homogeneous cantilever rods ($\overline{k_e} = 10$)

e_0a (nm)	Mode number	Ref. [13]		This study $\overline{K_0} = 10^{10}$&$\overline{K_L} = 10^{-10}$		
		Exact	FE	$n = 10$	$n = 30$	$n = 40$
1	1	3.5288	3.5289	3.54247	3.53341	3.53226
				$n = 50$	$n = 60$	$n = 100$
				3.53156	3.5311	3.53017
	2	5.5712	5.5765	$n = 10$	$n = 30$	$n = 40$
				5.64198	5.59518	5.58923
				$n = 50$	$n = 60$	$n = 100$
				5.58565	5.58326	5.57846

$$\overline{k_e} = \frac{k_e L^2}{\mu J} \tag{58}$$

$$\overline{K_0} = \frac{K_0 L}{\mu J} \tag{59}$$

$$\overline{K_L} = \frac{K_L L}{\mu J} \tag{60}$$

Here, $\overline{\omega}$ is the non-dimensional frequency, $\overline{k_e}$ is the elastic medium parameter. Lastly, $\overline{K_0}$ and $\overline{K_L}$ torsional spring parameters. Table 1 presents a comparison for homogeneous nanorods in the form of tubes with clamped support at both ends. The exact and FE (with 25 elements) results found by Numanoglu and Civalek [13] are given for all comparisons. In this study, the stiffnesses of the springs on both sides are chosen to be very large ($\overline{K_0} = \overline{K_L} = 10^{10}$) in order to fulfill the clamped support conditions of the nanorods. It is clear that this comparison of ten terms and twenty terms is perfectly harmonized. It is clear from this study that for nanorods with high stiffness, the result can be obtained even with low-term solutions.

Table 2 compares the dimensionless frequencies of a nanorod with one end clamped and the other end free. For a consistent comparison, the spring stiffness at one end of the nanotubes modeled in this study is set very high ($\overline{K_0} = 10^{10}$) while the spring stiffness at the other end is set very low ($\overline{K_L} = 10^{-10}$). It follows from this boundary condition that it is not possible to achieve perfect fits with low terms. Therefore, comparisons are made at various term numbers. The comparison is completed at one hundred terms, but it should be noted that increasing the number of terms further will increase the agreement even more.

As mentioned earlier, Numanoğlu and Civalek [13] also studied nanorods with a spring attachment on one side. The last comparison study is given via Table 3 and carried out for nanorods with one end clamped and the other end spring attached. Considering the two previous comparison studies, the number of terms is taken as one hundred. It is clear from the agreement that the model proposed in this study can be easily used in the torsional vibration analysis of nanorods with both deformable and rigid boundary conditions.

The main aim of this study, which is to analyze the torsional vibration of porous nanotubes under elastic boundary conditions based on NLET, has not been previously studied in the literature. The dimensionless vibration frequencies of three different nanotubes (two with pores and one without pores) are comparatively analyzed. Furthermore, FG nanotubes are considered surrounded by an elastic medium. How the composite nanotubes are affected by the material grading coefficient, pore coefficient, nonlocal parameter, stiffness of elastic springs and stiffness of the elastic medium will be investigated.

Table 3 Comparison of non-dimensional frequencies for homogeneous clamped and spring-attached rods ($\overline{k_e}$=0 & the first mode)

e_0a (nm)	Ref. [13]		This study
	Exact	FE	$K_0 = 10^{10} \& K_L = 5$
0	2.6537	2.6549	2.65468
1	2.6367	2.6379	2.63768
2	2.5870	2.5881	2.58782

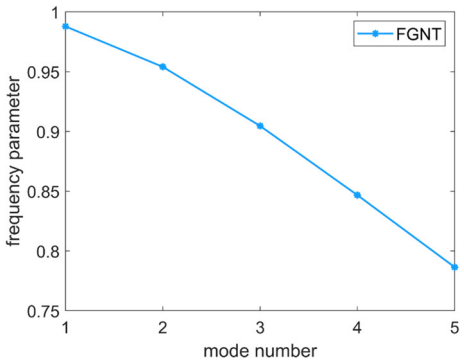

Fig. 4 NLET effect on the frequency parameter

The properties of the ceramic and metal phases that make up the composite NT in this study are as follows: $E_c = 151$ GPa, $E_m = 70$ GPa, $\rho_c = 3000\text{kg/m}^3$, $\rho_m = 2707\text{kg/m}^3$,$\upsilon_c = \upsilon_m = 0.3$. Also, geometical properties of the nanotubes are: $r_i = 1\text{nm}$, $r_o = 2\text{nm}$, $L = 10r_o$. In this study, frequency and some inputs are considered in the dimensionless form as follows:

$$\overline{\omega} = \omega L \sqrt{\frac{\rho_c}{\mu_c}} \tag{57}$$

$$\overline{k_e} = \frac{k_e L^2}{\mu_m J} \tag{58}$$

$$\overline{K_0} = \frac{K_0 L}{\mu_c J} \tag{59}$$

$$\overline{K_L} = \frac{K_L L}{\mu_c J} \tag{60}$$

It should be noted that $p = 1$, $\overline{K_0} = \overline{K_L} = 10^{10}$, $n = 20$, $e_0a = 1\text{nm}$, $\overline{k_e} = 10$ and $\vartheta = 0.1$ are used in the analyses presented in this work and first mode frequencies are analyzed unless otherwise stated. In Fig. 4, the change of frequency parameters of FGNT are plotted for the first five vibrational modes. The frequency parameter is calculated as follows:

$$\text{frequency parameter} = \frac{\text{frequency of NLET}}{\text{frequency of CET}} \tag{61}$$

Freqencies of NLET are obtained with $e_0a = 1$ nm. It is clear from this figure that NLET causes the frequencies to decrease. While the frequency parameters are close to 1 in the first mode, they start to decrease as the mode number increases. In other words, while the frequencies of NLET and CET are closer to each other in the first mode, the difference between them increases as the mode number increases. From this, it is understood that NLET is more effective in higher modes.

Figure 5 investigates the porosity effect for the nonlocal FG nanotubes. For this figure, pore coefficient is chosen as $\vartheta = 0.1$ for porous nanotubes. For non-porous nantubes, this parameter is equal to zero. From the figure, it is understood that the least frequencies are obtained for FGNT (non-porous case) and the highest frequencies are calculated for FGNT-I (evenly porous case). The decrease in the frequencies of the nanotubes caused by NLET can be easily seen in this example. As e_0a increases, dimensionless frequencies decrease. The increase in high e_0a values causes the frequencies to decrease more.

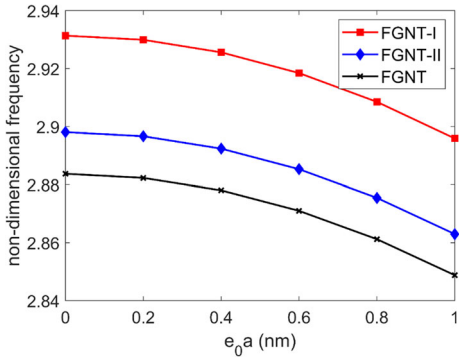

Fig. 5 Comparison of frequencies for different tube types

Figures 6a–c are drawn to compare the effects of NLET on porous and non-porous nanotubes. For this purpose, frequency ratios versus e_0a are shown. In this example, it is clear from the frequency parameters calculated with Eq. (61) that the effect of e_0a is almost the same for all three types of nanotubes studied.

Figures 7, 8, 9 shows the elastic medium effect for the nonlocal FGNT, FGNT-I and FGNT-II, respectively. For these figures, elastic medium parameter ($\overline{k_e}$) are chosen diferent five values for the three FG nanotubes. In these figures, in case of $\overline{k_e}$=0, solution gives the fequencies of non-embedded FG nanotube and it is understood that the lowest frequency values are obtained for this case. As elastic medium parameter is increased, the dimensionless torsional frequencies for nanotubes increase. It is also worth noting a remarkable result here. When the changes in non-dimensional frequencies are examined, it is concluded that the highest changes occur for FGNT-I, while the lowest changes occur for FGNT. In other words, the presence of the elastic medium or the increase in its rigidity affects FGNT-I the most. Non-porous FG nanotube is the type that is least affected by the presence of the elastic medium or the increase in its rigidity. It is also possible to once again compare the frequencies of FG nanotubes in this example. As can be seen, the highest dimensionless frequencies belong to FGNT-I.

In Fig. 10, non-dimensional frequencies are plotted against five different pore coefficients. $\overline{k_e} = 10$ is considered for this graph. The aim here is to show the effect of changing pore coefficient. The presence of pores increases the frequencies of FG nanotubes. The increase in the pore coefficient also causes a decrease in the material properties' values of the nanotube (such as Young's modulus, Poisson's ratio, and mass density). The increase in frequency that occurs as a result of the decrease in these properties' values can be explained by the rate at which the pore coefficient affects them. Since the pore in the cross-section causes the mass density of the nanotube to decrease much more, there is an increase in non-dimensional frequencies. It is clearly seen that the increase in pore coefficient affects the frequencies of FGNT-I more.

In Fig. 11, non-dimensional frequencies are shown versus five different material grading coefficients ($p = 0,\ 0.4,\ 0.8,\ 1.2,\ 1.6$). The purpose of this example is to investigate the effect of changing material grading coefficient. It is clear that for all three FG nanotubes, as the p value increases, there is a clear decrease in non-dimensional frequencies. It is worth emphasizing a point in this example, where the highest non-dimensional frequency values are obtained at $p = 0$. When $p = 0$, all three nanotubes take the form of porous and non-porous nanotubes consisting only of ceramic components. An increase in the p value means an increase in metallic properties, which causes a decrease in non-dimensional frequencies.

In Fig. 12, the variation of frequency parameters of FG nanotubes are plotted for the first five pore coefficients. For this example, the frequency parameter is calculated as follows:

$$\text{frequency parameter} = \frac{\text{frequency of} \overline{k_e} = 10}{\text{frequency of} \overline{k_e} = 0} \tag{62}$$

Freqencies of embedded nanotubes are obtained with $\overline{k_e} = 10$. The frequency-enhancing effect of the elastic medium is clear in Fig. 12. The purpose of this example is to reveal the relation between the elastic medium and the pore coefficient. The nanotube with the highest frequency parameter value means that it is most affected by the elastic medium. Here too, it is clear that FGNT-I is most affected by the presence of the elastic medium. As the porosity coefficient value increases for porous nanotubes, the frequency parameter value also increases. It is concluded from this that nanotubes begin to be more affected by the presence of the elastic medium as the pore rate increases.

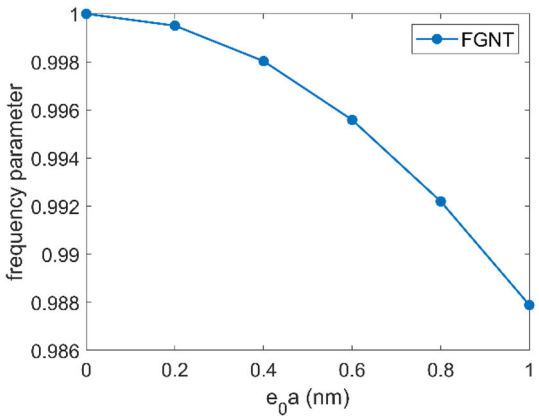

a) FGNT

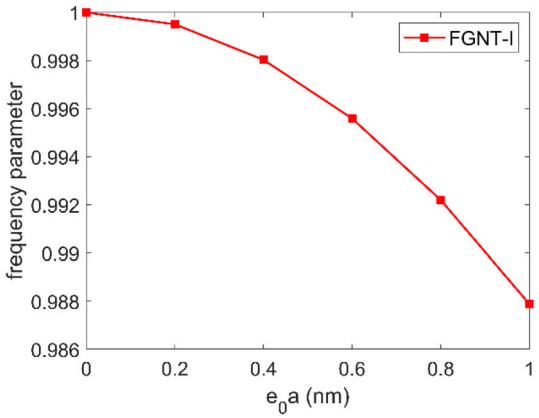

b) FGNT-I

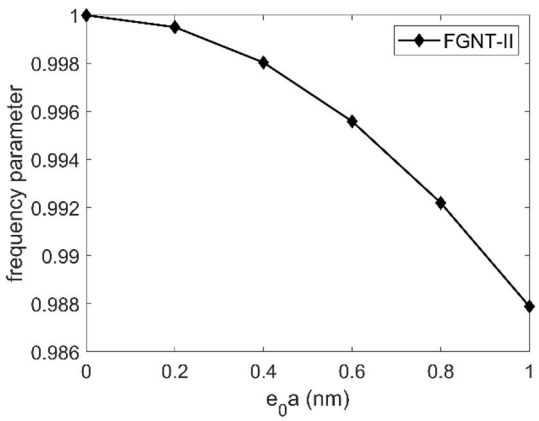

c) FGNT-II

Fig. 6 Comparison of frequency parameters for different tube types

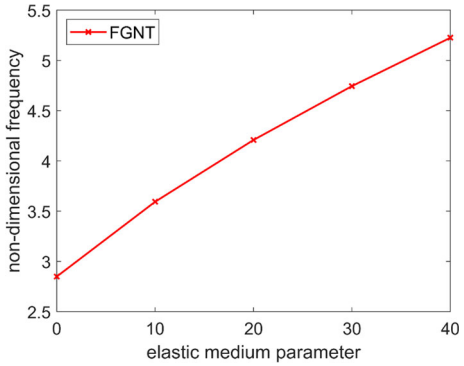

Fig. 7 Effect of $\overline{k_e}$ of the FGNT's non-dimensional frequencies

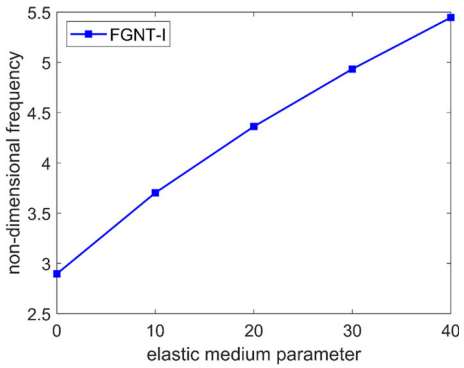

Fig. 8 Effect of $\overline{k_e}$ of the FGNT-I's non-dimensional frequencies

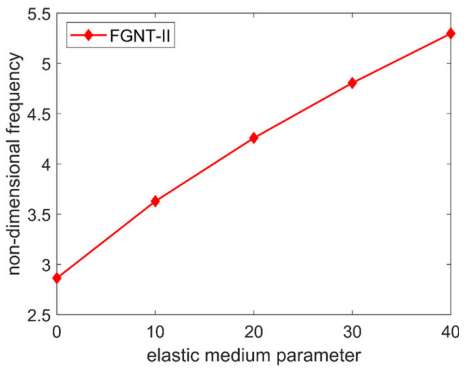

Fig. 9 Effect of $\overline{k_e}$ of the FGNT-II's non-dimensional frequencies

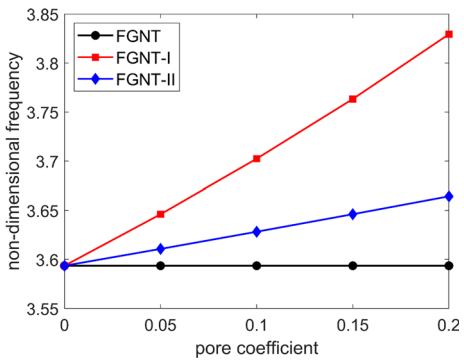

Fig. 10 Effect of ϑ on the non-dimensional frequencies

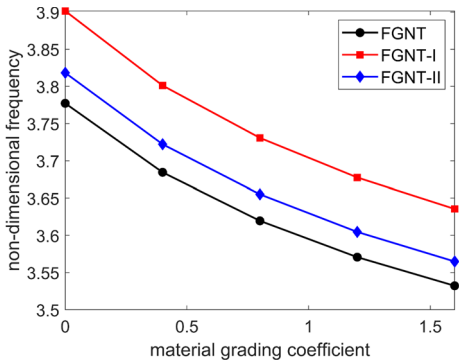

Fig. 11 Effect of p on the non-dimensional frequencies

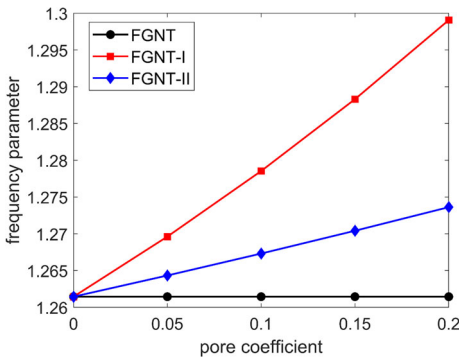

Fig. 12 Elastic medium effect on the frequency parameter

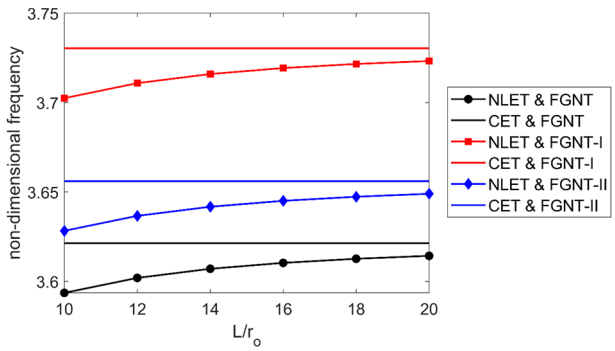

Fig. 13 Effect of length for NLET and CET

In Fig. 13, non-dimensional frequency values of FGNT, FGNT-I and FGNT-II based on various L/r_o values are plotted for both NLET and CET. In this example r_o is constant and the value of L is changed. In CET, the change in length has no effect on the frequencies, while in NLET, the change in length causes the frequencies to increase. For all three FG nanotubes, it is evident that as the length increases, the NLET and CET frequencies approach each other. This means that the nonlocality effect decreases as the length increases.

In Fig. 14, the effect of the torsional spring on the frequencies of the FG nanotubes is analyzed. For this, dimensionless frequencies are plotted against varying values of $\overline{K_0} = \overline{K_L}$. For all three nanotubes, it can be seen that as the torsional spring stiffness increases, the non-dimensional frequencies also increase. Also, the analysis shows that changes in the higher spring parameters affect the frequencies less. For this reason, at lower spring stiffnesses, the investigation steps are more frequent. It should be said here that one hundred terms are considered for this study.

Table 4 shows the frequencies of embedded and non-embedded FGNT-II for varying spring parameters. The aim here is to present how the change in spring parameters affects the NTs with and without elastic

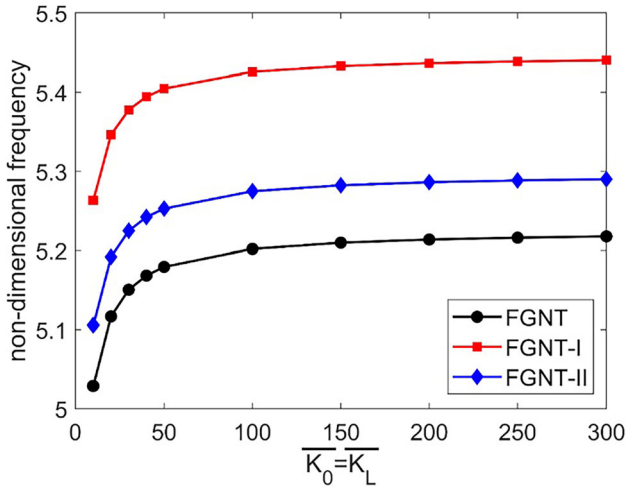

Fig. 14 Effect of torsinal spring prameters with equal stiffness ($\overline{k_e} = 40$)

Table 4 Effect of torsinal spring prameters on the embedded and non-embedded FGNT-II

$\overline{K_0} = \overline{K_L}$	Embedded FGNT-II	non-embedded FGNT-II	$\overline{K_0} = \overline{K_L}$	Embedded FGNT-II	non-embedded FGNT-II
10	5.10575	2.48950	100	5.27494	2.82028
20	5.19194	2.66179	150	5.28249	2.83437
30	5.22487	2.72548	200	5.28630	2.84147
40	5.24221	2.75857	250	5.28860	2.84574
50	5.25290	2.77883	300	5.29014	2.84860

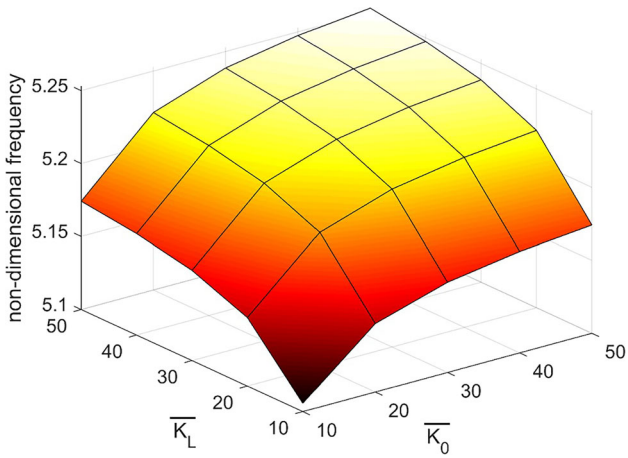

Fig. 15 Effect of torsinal spring prameters with different stiffnesses

medium. n=100 is considered for this study. For embedded FGNT-II, $\overline{k_e} = 40$ is taken. From the results in the table it can be easily understood that for non-embedded FGNT-II the variation of the spring parameters is of greater importance. This can be easily observed by the rate of increase in the dimensionless frequencies when $\overline{K_0} = \overline{K_L}$ are changed from 10 to 300.

In previous investigations, the stiffnesses of the torsional elastic springs of the FG nanotubes have been considered equal. However, an effective consequence of the solution method is that we are not constrained to take the spring parameters equal. We can obtain results by taking both spring stiffnesses differently. Figure 15 is intended to illustrate this feature. In this graph for FGNT-II, $\overline{k_e} = 40$ and 25 different combinations of spring parameters are considered with one hundred terms. With this example, it can be emphasized again that non-dimensional frequencies increment with increasing spring stiffness.

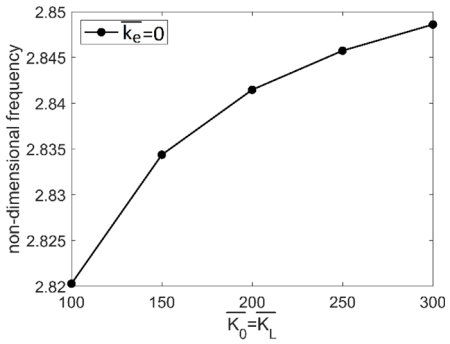

a) $\overline{k_e} = 0$

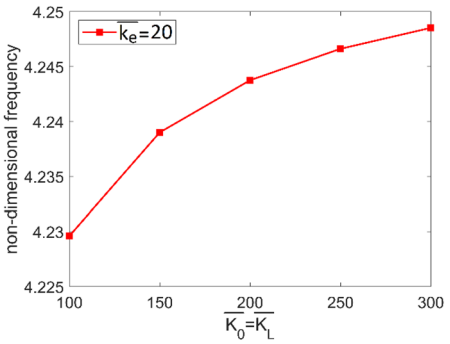

b) $\overline{k_e} = 20$

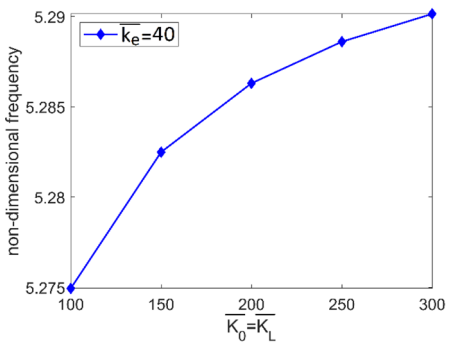

c) $\overline{k_e} = 40$

Fig. 16 Effect of torsinal spring prameters for various $\overline{k_e}$

In Fig. 16, the change of non-dimensional frequency values is plotted against different torsional spring parameters for various values of $\overline{k_e}$. The purpose of this graph drawn for FGNT-II is to show the relation between elastic medium and torsional spring parameters. In this example, where the solution is provided with $n = 100$, it can be emphasized once again that the increase in torsional spring parameters also increases the frequencies. On the other hand, the main conclusion to be drawn from this example is that when there is no elastic medium effect ($\overline{k_e} = 0$), the increase in torsional spring parameters affects the frequencies more. As $\overline{k_e}$ value increases, the effect of spring parameters on frequencies decreases.

6 Conclusion

In this study, NL free torsional vibration response of FG nanotubes embedded in an elastic matrix have been anticipated corresponding to various elastic or rigid boundary conditions and also patterns of porosity

dispersion. The main aim of this study is to investigate the size-dependent torsional vibration response of embedded FG porous NTs with deformable and un-deformable support conditions. A Fourier sine series in conjunction with the Stokes' transformation have been employed to obtain analytical expressions with power series for the nonlocal torsional vibration behaviours of FG porous nanotube embedded in an elastic matrix. Thereafter, a Fourier coefficient together with the force boundary conditions are employed to express the eigenvalue problem. Looking at the results obtained in the study, it is understood that the presence of pores affects the frequencies of the functionally graded nanotubes. This effect occurs at different rates depending on the type of porosity distribution. Nonlocality and elastic medium effects decrease and increase frequencies, respectively. The elastic medium effect strengthens the FG nanotube, causing the frequencies to increase. Increasing the material grading coefficient directs the FG nanotube from the ceramic dominant form to the metal dominant form, causing the frequencies to decrease. It can be seen that by increasing the rigidity of torsional springs, the free torsional vibration frequencies of FG porous/non-porous NTs increase. Adjusting these springs to equal or different stiffness can be beneficial in terms of frequency control.

Author contributions B.U.: conceptualization, formal analysis, methodology, visualization, writing-review & editing M.Ö.Y.: conceptualization, formal analysis, methodology, visualization, writing-review & editing Ö.C.: conceptualization, formal analysis, methodology, visualization, writing-review & editing

Funding Open access funding provided by the Scientific and Technological Research Council of Türkiye (TÜBİTAK).

Declarations

Conflict of interest The authors declared no potential conflict of interest with respect to the research, authorship, and/or publication of this article.

References

1. Wang, S.S.: Fracture mechanics for delamination problems in composite materials. J. Compos. Mater. **17**(3), 210–223 (1983)
2. Shanmugavel, P.G.B.B., Bhaskar, G.B., Chandrasekaran, M., Mani, P.S., Srinivasan, S.P.: An overview of fracture analysis in functionally graded materials. Eur. J. Sci. Res. **68**(3), 412–439 (2012)
3. Mahamood, R. M., Akinlabi, E. T., Shukla, M., & Pityana, S. L. (2012). Functionally graded material: an overview.
4. Chen, D., Gao, K., Yang, J., Zhang, L.: Functionally graded porous structures: analyses, performances, and applications–a review. Thin-Wall. Struct. **191**, 111046 (2023)
5. Mindlin, R.D.: Micro-structure in linear elasticity. Arch. Ration. Mech. Anal. **16**, 51–78 (1964)
6. Mindlin, R.D.: Second gradient of strain and surface-tension in linear elasticity. Int. J. Solids Struct.Struct. **1**(4), 417–438 (1965)
7. Lim, C.W., Zhang, G., Reddy, J.N.: A higher-order nonlocal elasticity and strain gradient theory and its applications in wave propagation. J. Mech. Phys. Solids **78**, 298–313 (2015)
8. Eringen, A.C., Edelen, D.G.B.: On nonlocal elasticity. Int. J. Eng. Sci. **10**(3), 233–248 (1972)
9. Eringen, A.C.: Nonlocal polar elastic continua. Int. J. Eng. Sci. **10**(1), 1–16 (1972)
10. Eringen, A.C.: On differential equations of nonlocal elasticity and solutions of screw dislocation and surface wave. J. Appl. Phys. **54**, 4703–4710 (1983)
11. Yang, F., Chong, A.C.M., Lam, D.C.C., Tong, P.: Couple stress based strain gradient theory for elasticity. Int. J. Solids Struct.Struct. **39**(10), 2731–2743 (2002)
12. Toupin, R.A.: Elastic materials with couple-stresses. Arch. Ration. Mech. Anal. **11**, 385–414 (1962)
13. Numanoğlu, H.M., Civalek, Ö.: On the torsional vibration of nanorods surrounded by elastic matrix via nonlocal FEM. Int. J. Mech. Sci. **161**, 105076 (2019)
14. Civalek, Ö., Uzun, B., Yayli, M.Ö.: Torsional vibrations of functionally graded restrained nanotubes. Eur. Phys. J. Plus **137**(1), 113 (2022)
15. Loya, J.A., Aranda-Ruiz, J.A., Fernández-Sáez, J.: Torsion of cracked nanorods using a nonlocal elasticity model. J. Phys. D Appl. Phys. **47**(11), 115304 (2014)
16. Uzun, B., Kafkas, U., Deliktaş, B., Yaylı, M.Ö.: Size-dependent vibration of porous bishop nanorod with arbitrary boundary conditions and nonlocal elasticity effects. J. Vibr. Eng. & Technol. **11**(3), 809–826 (2023)

17. Civalek, Ö., Uzun, B., Yaylı, M.Ö.: An effective analytical method for buckling solutions of a restrained FGM nonlocal beam. Comput. Appl. Math. Appl. Math. **41**(2), 67 (2022)
18. Numanoğlu, H.M., Ersoy, H., Akgöz, B., Civalek, Ö.: A new eigenvalue problem solver for thermo-mechanical vibration of Timoshenko nanobeams by an innovative nonlocal finite element method. Math. Methods Appl. Sci. **45**(5), 2592–2614 (2022)
19. Demir, C., Civalek, O.: On the analysis of microbeams. Int. J. Eng. Sci. **121**, 14–33 (2017)
20. Janghorban, M.: Two different types of differential quadrature methods for static analysis of microbeams based on nonlocal thermal elasticity theory in thermal environment. Arch. Appl. Mech. **82**(5), 669–675 (2012)
21. Preethi, K., Raghu, P., Rajagopal, A., Reddy, J.N.: Nonlocal nonlinear bending and free vibration analysis of a rotating laminated nano cantilever beam. Mech. Adv. Mater. Struct.Struct. **25**(5), 439–450 (2018)
22. Eltaher, M.A., Shanab, R.A., Mohamed, N.A.: Analytical solution of free vibration of viscoelastic perforated nanobeam. Arch. Appl. Mech. **93**(1), 221–243 (2023)
23. Khosravi, F., Hosseini, S.A., Hamidi, B.A., Dimitri, R., Tornabene, F.: Nonlocal torsional vibration of elliptical nanorods with different boundary conditions. Vibration **3**(3), 189–203 (2020)
24. Gholami, M., Zare, E., Alibazi, A.: Applying Eringen's nonlocal elasticity theory for analyzing the nonlinear free vibration of bidirectional functionally graded Euler-Bernoulli nanobeams. Arch. Appl. Mech. **91**(7), 2957–2971 (2021)
25. Narendar, S.: Spectral finite element and nonlocal continuum mechanics based formulation for torsional wave propagation in nanorods. Finite Elem. Anal. Des. **62**, 65–75 (2012)
26. Khosravi, F., Hosseini, S.A., Hamidi, B.A.: Analytical investigation on free torsional vibrations of noncircular nanorods. J. Braz. Soc. Mech. Sci. Eng. **42**(10), 514 (2020)
27. Jalaei, M.H., Thai, H.T., Civalek, Ö: On viscoelastic transient response of magnetically imperfect functionally graded nanobeams. Int. J. Eng. Sci. **172**, 103629 (2022)
28. Arefi, M., Kiani, M., Rabczuk, T.: Application of nonlocal strain gradient theory to size dependent bending analysis of a sandwich porous nanoplate integrated with piezomagnetic face-sheets. Compos. B Eng. **168**, 320–333 (2019)
29. Abouelregal, A.E., Marin, M.: The response of nanobeams with temperature-dependent properties using state-space method via modified couple stress theory. Symmetry **12**(8), 1276 (2020)
30. Civalek, O., Uzun, B., Yayli, M.O.: A Fourier sine series solution of static and dynamic response of nano/micro-scaled FG rod under torsional effect. Adv. Nano Res **12**(5), 467–482 (2022)
31. Yin, B., Fang, J.: Modified couple stress-based free vibration and dynamic response of rotating FG multilayer composite microplates reinforced with graphene platelets. Arch. Appl. Mech. **93**(3), 1051–1079 (2023)
32. Liu, C., Yu, J., Xu, W., Zhang, X., Wang, X.: Dispersion characteristics of guided waves in functionally graded anisotropic micro/nano-plates based on the modified couple stress theory. Thin-Walled Struct. **161**, 107527 (2021)
33. Uzun, B., Yaylı, M.Ö.: Porosity dependent torsional vibrations of restrained FG nanotubes using modified couple stress theory. Mater. Today Commun. **32**, 103969 (2022)
34. Liu, J., Peng, Y.: Complementary energy principle associated with modified couple stress theory for Euler micro-beams considering support movements and negative Poisson's ratio. Arch. Appl. Mech. **92**(7), 2119–2135 (2022)
35. Kim, J., Zur, K.K., Reddy, J.N.: Bending, free vibration, and buckling of modified couples stress-based functionally graded porous micro-plates. Compos. Struct.Struct. **209**, 879–888 (2019)
36. Kiani, K.: Nonlocal continuum-based modeling of a nanoplate subjected to a moving nanoparticle. Part I: Theoretical formulations. Phys. E Low-Dimensional Syst. Nanostruct. **44**(1), 229–248 (2011)
37. Shirai, Y., Osgood, A.J., Zhao, Y., Kelly, K.F., Tour, J.M.: Directional control in thermally driven single-molecule nanocars. Nano Lett. **5**(11), 2330–2334 (2005)
38. Shirai, Y., Osgood, A.J., Zhao, Y., Yao, Y., Saudan, L., Yang, H., Yu-Hung, C., Alemany, L.B., Sasaki, T., Morin, J.F., Guerrero, J.M.: Surface-rolling molecules. J. Am. Chem. Soc. **128**(14), 4854–4864 (2006)
39. Morin, J.F., Shirai, Y., Tour, J.M.: En route to a motorized nanocar. Org. Lett. **8**(8), 1713–1716 (2006)
40. Arani, A.G., Roudbari, M.A., Amir, S.: Nonlocal vibration of SWBNNT embedded in bundle of CNTs under a moving nanoparticle. Phys. B B **407**(17), 3646–3653 (2012)
41. Cho, J., Luo, J.J., Daniel, I.M.: Mechanical characterization of graphite/epoxy nanocomposites by multi-scale analysis. Compos. Sci. Technol. **67**, 2399–2407 (2007)
42. Tsai, J.L., Tu, J.F.: Characterizing mechanical properties of graphite using molecular dynamic simulation. Mater. Des. **31**, 194–199 (2010)
43. Wu, H.A.: Molecular dynamics simulation of loading rate and surface effects on the elastic bending behavior of metal nanorod. Comput. Mater. Sci. Mater. Sci. **31**, 287–291 (2004)
44. Yakobson, B.I., Brabec, C.J., Bernholc, J.: Nanomechanics of carbon tubes: instabilities beyond linear response. Phys. Rev. Lett. **76**, 2511–2514 (1996)
45. Lu, J.M., Wang, Y.C., Chang, J.G., Su, M.H., Hwang, C.C.: Molecular-dynamic investigation of buckling of double-walled carbon nanotubes under uniaxial compression. J. Phys. Soc. Jpn.Jpn. **77**, 044603 (2008)
46. Aydogdu, M., Filiz, S.: Modeling carbon nanotube-based mass sensors using axial vibration and nonlocal elasticity. Physica E E **43**(6), 1229–1234 (2011)
47. Aydogdu, M.: A nonlocal rod model for axial vibration of double-walled carbon nanotubes including axial van der Waals force effects. J. Vib. ControlVib. Control **21**(16), 3132–3154 (2015)
48. Natsuki, T., Shi, J.X., Ni, Q.Q.: Vibration analysis of nanomechanical mass sensor using double-layered graphene sheets resonators. J. Appl. Phys. **114**(9), 094307 (2013)
49. Song, M., Kitipornchai, S., Yang, J.: Free and forced vibrations of functionally graded polymer composite plates reinforced with graphene nanoplatelets. Compos. Struct.Struct. **159**, 579–588 (2017)
50. Atanasov, M.S., Karličić, D., Kozić, P.: Forced transverse vibrations of an elastically connected nonlocal orthotropic double-nanoplate system subjected to an in-plane magnetic field. Acta Mech. Mech. **228**, 2165–2185 (2017)
51. Li, L., Hu, Y.: Torsional vibration of bi-directional functionally graded nanotubes based on nonlocal elasticity theory. Compos. Struct.Struct. **172**, 242–250 (2017)

52. Li, L., Hu, Y.: Torsional statics of two-dimensionally functionally graded microtubes. Mech. Adv. Mater. Struct.Struct. **26**(5), 430–442 (2019)
53. Chang, X., Zhou, J.: Static and dynamic characteristics of post-buckling of porous functionally graded pipes under thermal shock. Compos. Struct.Struct. **288**, 115373 (2022)
54. She, G.L., Yuan, F.G., Ren, Y.R., Xiao, W.S.: On buckling and postbuckling behavior of nanotubes. Int. J. Eng. Sci. **121**, 130–142 (2017)
55. Wattanasakulpong, N., Chaikittiratana, A.: Flexural vibration of imperfect functionally graded beams based on Timoshenko beam theory: chebyshev collocation method. Meccanica **50**, 1331–1342 (2015)
56. Wattanasakulpong, N., Ungbhakorn, V.: Linear and nonlinear vibration analysis of elastically restrained ends FGM beams with porosities. Aerosp. Sci. Technol. Sci. Technol. **32**(1), 111–120 (2014)
57. Turan, M.: Fonksiyonel Derecelendirilmiş Gözenekli Kirişlerin Sonlu Elemanlar Yöntemiyle Statik Analizi. Mühendislik Bilimleri ve Tasarım Dergisi **10**(4), 1362–1374 (2022)
58. Karlicic, D., Murmu, T., Adhikari, S., McCarthy, M.: Nonlocal structural mechanics. John Wiley & Sons (2015)
59. Taati, E., Borjalilou, V., Fallah, F., Ahmadian, M.T.: On size-dependent nonlinear free vibration of carbon nanotube-reinforced beams based on the nonlocal elasticity theory: Perturbation technique. Mech. Based Des. Struct. Machines **50**(6), 2124–2146 (2022)
60. Kafkas, U. (2022). Dönel Yaylar Ile Sabitlenmiş Bir Karbon Nanotüpün Boşluk Oranına Bağlı Serbest Titreşim Analizi [Doktora Tezi]. Bursa Uludağ Üniversitesi.
61. Arghavan, S., Hematiyan, M.R.: Torsion of functionally graded hollow tubes. Eur. J. Mech.-A/Solids **28**(3), 551–559 (2009)
62. Polyzos, D., Huber, G., Mylonakis, G., Triantafyllidis, T., Papargyri-Beskou, S., Beskos, D.: Torsional vibrations of a column of fine-grained material: a gradient elastic approach. J. Mech. Phys. Solids **76**, 338–358 (2015)
63. Reddy, J.N.: Energy principles and variational methods in applied mechanics, 2nd edn. John Wiley & Sons, New York (2002)
64. El-Borgi, S., Rajendran, P., Friswell, M.I., Trabelssi, M., Reddy, J.N.: Torsional vibration of size-dependent viscoelastic rods using nonlocal strain and velocity gradient theory. Compos. Struct.Struct. **186**, 274–292 (2018)
65. Abouelregal, A.E., Akgöz, B., Civalek, Ö.: Magneto-thermoelastic interactions in an unbounded orthotropic viscoelastic solid under the Hall current effect by the fourth-order Moore-Gibson-Thompson equation. Comput. Math. Appl.. Math. Appl. **141**, 102–115 (2023)
66. Saimi, A., Bensaid, I., Fellah, A.: Effect of crack presence on the dynamic and buckling responses of bidirectional functionally graded beams based on quasi-3D beam model and differential quadrature finite element method. Arch. Appl. Mech. **93**(8), 3131–3151 (2023)
67. Awrejcewicz, J., Krysko, A.V., Mrozowski, J., Saltykova, O.A., Zhigalov, M.V.: Analysis of regular and chaotic dynamics of the Euler-Bernoulli beams using finite difference and finite element methods. Acta Mech. Sin. Mech. Sin. **27**, 36–43 (2011)
68. Sharifi, P., Shojaee, M., Salighe, S.: Vibration of rotating porous nanocomposite eccentric semi-annular and annular plates in uniform thermal environment using TDQM. Arch. Appl. Mech. **93**(4), 1579–1604 (2023)
69. Trabelssi, M., El-Borgi, S., Friswell, M.I.: A high-order FEM formulation for free and forced vibration analysis of a nonlocal nonlinear graded Timoshenko nanobeam based on the weak form quadrature element method. Arch. Appl. Mech. **90**, 2133–2156 (2020)
70. Challamel, N., Picandet, V., Elishakoff, I., Wang, C.M., Collet, B., Michelitsch, T.: On nonlocal computation of eigenfrequencies of beams using finite difference and finite element methods. Int. J. Struct. Stab. Dyn.Struct. Stab. Dyn. **15**(07), 1540008 (2015)
71. Wang, S.M., Ni, Y.Q., Duan, Y.F., Yau, J.D.: Vector form intrinsic finite element method for stochastic analysis of train—track–bridge coupling system. Int. J. Struct. Stab. Dyn.Struct. Stab. Dyn. **21**(14), 2140012 (2021)
72. Zenkour, A.M., Abbas, I.A.: Nonlinear transient thermal stress analysis of temperature-dependent hollow cylinders using a finite element model. Int. J. Struct. Stab. Dyn.Struct. Stab. Dyn. **14**(07), 1450025 (2014)
73. Taghizadeh, M., Ovesy, H.R., Ghannadpour, S.A.M.: Beam buckling analysis by nonlocal integral elasticity finite element method. Int. J. Struct. Stab. Dyn.Struct. Stab. Dyn. **16**(06), 1550015 (2016)
74. Salah, M., Matbuly, M.S., Civalek, O., Ragb, O.: Calculation of four-dimensional unsteady gas flow via different quadrature schemes and Runge-Kutta 4th ordermethod. Adv. Appl. Math. Mech. **15**, 1–22 (2023)